Anaerobic peroxisomes in *Mastigamoeba balamuthi*

Tien Le[a], Vojtěch Žárský[a], Eva Nývltová[a], Petr Rada[a], Karel Harant[a], Marie Vancová[b], Zdeněk Verner[a], Ivan Hrdý[a], and Jan Tachezy[a,1]

[a]Department of Parasitology, Faculty of Science, BIOCEV, Charles University, 25242 Vestec, Czech Republic; and [b]Institute of Parasitology, Biology Centre, Czech Academy of Sciences, 370 05 České Budějovice, Czech Republic

Edited by Tom M. Fenchel, University of Copenhagen, Helsingor, Denmark, and approved December 12, 2019 (received for review July 3, 2019)

The adaptation of eukaryotic cells to anaerobic conditions is reflected by substantial changes to mitochondrial metabolism and functional reduction. Hydrogenosomes belong among the most modified mitochondrial derivative and generate molecular hydrogen concomitant with ATP synthesis. The reduction of mitochondria is frequently associated with loss of peroxisomes, which compartmentalize pathways that generate reactive oxygen species (ROS) and thus protect against cellular damage. The biogenesis and function of peroxisomes are tightly coupled with mitochondria. These organelles share fission machinery components, oxidative metabolism pathways, ROS scavenging activities, and some metabolites. The loss of peroxisomes in eukaryotes with reduced mitochondria is thus not unexpected. Surprisingly, we identified peroxisomes in the anaerobic, hydrogenosome-bearing protist *Mastigamoeba balamuthi*. We found a conserved set of peroxin (Pex) proteins that are required for protein import, peroxisomal growth, and division. Key membrane-associated Pexs (*Mb*Pex3, *Mb*Pex11, and *Mb*Pex14) were visualized in numerous vesicles distinct from hydrogenosomes, the endoplasmic reticulum (ER), and Golgi complex. Proteomic analysis of cellular fractions and prediction of peroxisomal targeting signals (PTS1/PTS2) identified 51 putative peroxisomal matrix proteins. Expression of selected proteins in *Saccharomyces cerevisiae* revealed specific targeting to peroxisomes. The matrix proteins identified included components of acyl-CoA and carbohydrate metabolism and pyrimidine and CoA biosynthesis, whereas no components related to either β-oxidation or catalase were present. In conclusion, we identified a subclass of peroxisomes, named "anaerobic" peroxisomes that shift the current paradigm and turn attention to the reductive evolution of peroxisomes in anaerobic organisms.

peroxisome | *Mastigamoeba balamuthi* | mitochodria | anaerobiosis

Peroxisomes are single membrane-bound organelles present in nearly all eukaryotes (1). They are defined by a conserved set of proteins named peroxins (Pexs) that are required for peroxisomal biogenesis (2). Biochemically, most peroxisomes share the function of fatty acid oxidation, which generates hydrogen peroxide, and hydrogen peroxide-degrading enzymes, namely, catalase, to prevent cellular oxidative damage (3). Additional peroxisomal pathways are highly variable, indicating the remarkable versatility of peroxisomal functions (4). This is reflected by the various names of peroxisomal subtypes, such as glyoxysomes, glycosomes, and Woronin bodies (5). The need for the compartmentalization of enzymes that produce reactive oxygen species (ROS) has been proposed as a driving force behind the evolution of peroxisomes. Peroxisomes were most likely derived from the endoplasmic reticulum (ER) and originated endogenously within eukaryotes (6, 7), although they were long thought to be endosymbiotic remnants similar to mitochondria and plastids (8). The β-oxidation of fatty acids is considered to be the earliest pathway that resided in an ancestral peroxisomal proteome due to its widespread occurrence (6). Phylogenetic analysis suggested that this pathway was inherited from the endosymbiotic ancestor of mitochondria, duplicated and retargeted to peroxisomes to minimize the harmful effects of ROS (6, 7). However, a parallel role of the ER in the evolution of peroxisomal β-oxidation has been proposed (9, 10).

In addition to fatty acid metabolism, there is a plethora of other metabolic, regulatory, and evolutionary links between peroxisomes and mitochondria (11, 12). For example, the glyoxylate cycle of peroxisomes of land plants, fungi, alveolates, and lower animals uses acetyl-CoA as a substrate to produce succinate that can be imported into mitochondria to replenish the tricarboxylic acid (TCA) cycle. Both peroxisomes and mitochondria divide by fission and share multiple components of the fission machinery (13). More recently, mitochondria appeared to be directly involved in peroxisome biogenesis as a source of peroxisomal membranes and membrane proteins (14). Because of this tight interplay between peroxisomes and mitochondria and the dependence of key peroxisomal oxidases on the presence of molecular oxygen, it is not surprising that peroxisomes are generally absent in anaerobic unicellular eukaryotes (protists) (15, 16). These eukaryotes harbor highly reduced anaerobic mitochondria, such as hydrogenosomes and mitosomes (17). Hydrogenosomes lack most mitochondrial metabolic functions, including β-oxidation. ATP is generated at the substrate level using an anaerobic pathway that catabolizes pyruvate or malate to acetate, CO_2, and molecular hydrogen. Anaerobic conditions apparently prevent the use of oxygen-dependent β-oxidation of fatty acid metabolism in both peroxisomes and mitochondria, as well as other oxygen-dependent catabolic

Significance

It is generally accepted that peroxisomes are absent in anaerobic eukaryotes. These organelles have evolved to compartmentalize oxidative pathways and prevent cellular oxidative damage, namely, the β-oxidation of fatty acids that utilizes molecular oxygen and produces hydrogen peroxide. Mitochondria possess a parallel β-oxidation pathway coupled with the respiratory chain. The adaptation of eukaryotes to anaerobiosis is reflected by the reduction of mitochondrial metabolism and, not surprisingly, concomitant loss of peroxisomes. The free-living anaerobic protist *Mastigamoeba balamuthi* is an organism that contradicts this paradigm. Although *Mastigamoeba* possesses hydrogenosomes, an anaerobic form of mitochondria, it also harbors peroxisomes. These organelles contain the archetypical Pexs that are required for peroxisomal biogenesis; however, they lack the hallmarks of peroxisomal metabolism, β-oxidation and catalase.

Author contributions: J.T. designed research; T.L., V.Ž., E.N., P.R., K.H., M.V., Z.V., I.H., and J.T. performed research; and J.T. wrote the paper.

The authors declare no competing interest.

This article is a PNAS Direct Submission.

Data deposition: MaxQuant results were uploaded to the PRIDE partner repository (https://www.ebi.ac.uk/pride/archive/) with the dataset identifier PXD014205. The sequences reported in this paper have been deposited in the online resource for community annotation of eukaryotes (ORCAE, https://bioinformatics.psb.ugent.be/orcae/) and are given in Dataset S1.

[1]To whom correspondence may be addressed. Email: tachezy@natur.cuni.cz.

This article contains supporting information online at https://www.pnas.org/lookup/suppl/doi:10.1073/pnas.1909755117/-/DCSupplemental.

and biosynthetic pathways in anaerobic protists. As a consequence, peroxisomes may become dispensable for these organisms.

Mastigamoeba balamuthi is a free-living anaerobic amoeba of the Archamoebae lineage. The characteristics of the mitochondria of *M. balamuthi* conform to those of hydrogenosomes (18). The anaerobic character of *M. balamuthi* emphasizes the presence of a nitrogen-fixing (NIF) and oxygen-sensitive ε-bacterial FeS cluster assembly machinery that replaced the standard mitochondrial iron–sulfur cluster (ISC) machinery (19). Moreover, oxygen-sensitive enzymes such as hydrogenases are present in *M. balamuthi* hydrogenosomes and in the cytosol, producing hydrogen from both compartments (19). Archamoebae belongs to the group Conosa with the sister lineage Mycetozoa that inhabits aerobic niches and contains oxygen-respiring mitochondria and standard peroxisomes (20, 21). Thus, it is likely that hydrogenosomes in *M. balamuthi* evolved from aerobic mitochondria via secondary adaptation to anaerobic environments, and we expected that an anaerobic lifestyle would lead to the loss of peroxisomes, as observed in other anaerobic protists. To our surprise, we found that *M. balamuthi* retains a full set of Pexs to form peroxisomes, and we identified enzymes that are delivered to the peroxisomal matrix via typical peroxisomal targeting signals (PTSs) to catalyze fragmented metabolic pathways. However, the oxygen-dependent peroxisomal hallmarks, including β-oxidation of fatty acids and catalase, are absent. These organelles represent a peroxisomal subtype named anaerobic peroxisomes.

Results

Identification and Cell Localization of Pexs. Analysis of the *M. balamuthi* genome sequence using HHpred searches indicated the presence of genes encoding a set of 14 Pexs involved in the recognition of PTS1 and PTS2 (Pex5 and 7, respectively), protein docking and import (Pex13 and 14), receptor recycling (Pex1, 2, 6, 10, and 12), membrane protein targeting (Pex3, 16, and 19), and peroxisome fission (Pex11-1 and Pex11-2) (Fig. 1*A* and *SI Appendix*, Fig. S1 and Table S1). Most *M. balamuthi* Pexs (*Mb*Pexs) were colinear or slightly shorter than the corresponding orthologs, and all possessed the expected functional domains (*SI Appendix*, Fig. S2). The C-terminal domain of Pex14 is markedly short; however, its N-terminal domain contains characteristic phenylalanine residues that are indispensable for its interaction with Pex5 (22) (*SI Appendix*, Fig. S2). The functional domains were identified using HHpred searches with high confidence (probability values ranged from 84 to 100) (*SI Appendix*, Fig. S2), whereas the overall similarity of *Mb*Pex protein sequences to their human orthologs ranged between 14% for Pex3 and 57% for Pex7 (*SI Appendix*, Table S2). The correct identification of *Mb*Pexs containing domains that are present in various proteins with unrelated functions, such as ATPases associated with diverse cellular activities (AAA, Pex1, and Pex6), tetratricopeptide repeats (TPR and Pex5), WD40 repeats (Pex7), and proteins of the RING family (Pex2, Pex10, and Pex12), was supported by phylogenetic analysis using human, yeast, and *Dictyostelium discoideum* orthologs and selected outgroups (Fig. 1*B*). Phylogenetic analysis of the *Mb*Pex11-1 and *Mb*Pex11-2 paralogs revealed their relationships with mammalian Pex11α and Pex11γ, respectively (*SI Appendix*, Table S2 and Fig. S3). These proteins are involved in the recruitment of the peroxisomal membrane fission machinery, as are Fis1, Mff, and DRP1 (23, 24). Indeed, our searches identified genes for Fis1 (m51a1_g2061) and DRP1 (m51a1_g631) in the *M. balamuthi* genome, which supports the predicted function of *Mb*Pex11-1 and *Mb*Pex11-2.

The *Mb*Pex5 receptor contains a conserved Cys-13 residue that is required for ubiquitination by the E2 ubiquitin-conjugating enzyme Pex4 (25) and thus receptor recycling (*SI Appendix*, Fig. S2). In *M. balamuthi*, we identified neither Pex4 nor the Pex4-anchoring

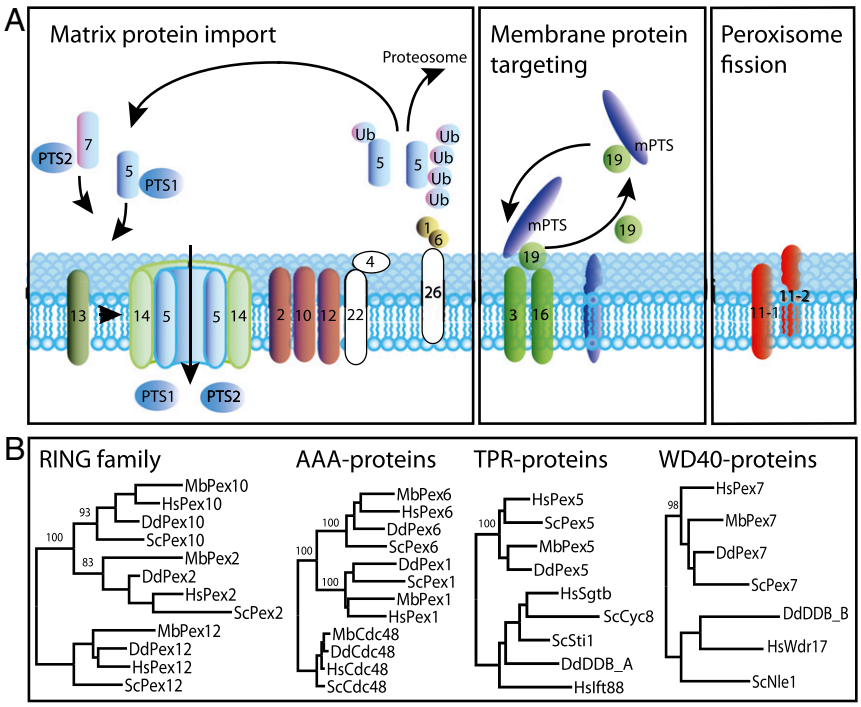

Fig. 1. (*A*) Scheme of the peroxisomal machinery identified in *M. balamuthi*. The white color indicates Pexs that were not identified in *M. balamuthi*. (*B*) Phylogenetic analysis of selected proteins was performed to discriminate peroxins (Pexs) and proteins that share common domains, including ATPases associated with diverse cellular activities (AAA, Pex1, and Pex6), tetratricopeptide repeats (TPR and Pex5), WD40 repeats (Pex7), and proteins of the RING family (Pex2, Pex10, and Pex12). Mb, *M. balamuthi*; Hs, *Homo sapiens*; Dd, *Dictyostelium discoideum*; Sc, *Saccharomyces cerevisiae*. Accession numbers are given in *SI Appendix*, Fig. S2 and Table S1.

protein Pex22 (Fig. 1*A*). Moreover, Pex26, which anchors the Pex1/6 complex, seems to be absent as well. However, Pex4, Pex22, and Pex26 are not generally distributed in eukaryotes (*SI Appendix*, Fig. S1). For example, Pex4 and Pex22 are absent in metazoans, and Pex22 is absent in diatoms, whereas metazoan Pex26 is replaced by Pex15 in *Saccharomyces cerevisiae* (26), and Pex26 is absent in kinetoplastids and diatoms (*SI Appendix*, Fig. S1) (27).

To validate our in silico predictions, we investigated the cellular localization of membrane-associated *Mb*Pexs. Confocal immunofluorescence microscopy (IF) using specific polyclonal antibodies (Abs) raised against *Mb*Pex3, *Mb*Pex11-1, and *Mb*Pex14 labeled numerous small vesicles scattered within the *M. balamuthi* cytosol. Importantly, *Mb*Pex14 colocalized in the same vesicles with *Mb*Pex3 (Pearson's correlation coefficient [PCC] $r = 0.85$) as well as with *Mb*Pex11 (PCC $r = 0.86$) (Fig. 2*A*). To further support the specific localization of Pexs and to estimate the size and shape of putative peroxisomes and their relationships with other organelles, we subjected *M. balamuthi* to stimulated emission depletion (STED) and immunoelectron microscopy analysis (Fig. 2 *B* and *C*). Dual-color STED imaging not only confirmed the colocalization of Pex3 and Pex14 signals but also enabled the observation of separate Pex3 and Pex14 signals that were localized in close proximity, suggesting a heterogeneous distribution of Pex3 and Pex14 across the organelles (Fig. 2*B*), as reported for Pexs in peroxisomes of human fibroblasts (28). Pex3/Pex14-labeled vesicles appeared mostly as circular, elliptical, or elongated structures. Their sizes ranged from a minimum of 80 nm (circular structures) to a maximum of 440 nm (elongated structures), and the average area of labeled vesicles was $0.013 \pm 0.009\ \mu m^2$ (mean ± SD, $n = 176$). Pex11-1–labeled vesicles were considerably smaller than hydrogenosomes visualized with antisuccinate dehydrogenase subunit B (SdhB) Ab (Fig. 2*B*). Neither hydrogenosomes nor ER structures and vesicles of the unstacked Golgi apparatus (29) colocalized with Pex11-1–labeled vesicles. Immunoelectron microscopy indicated

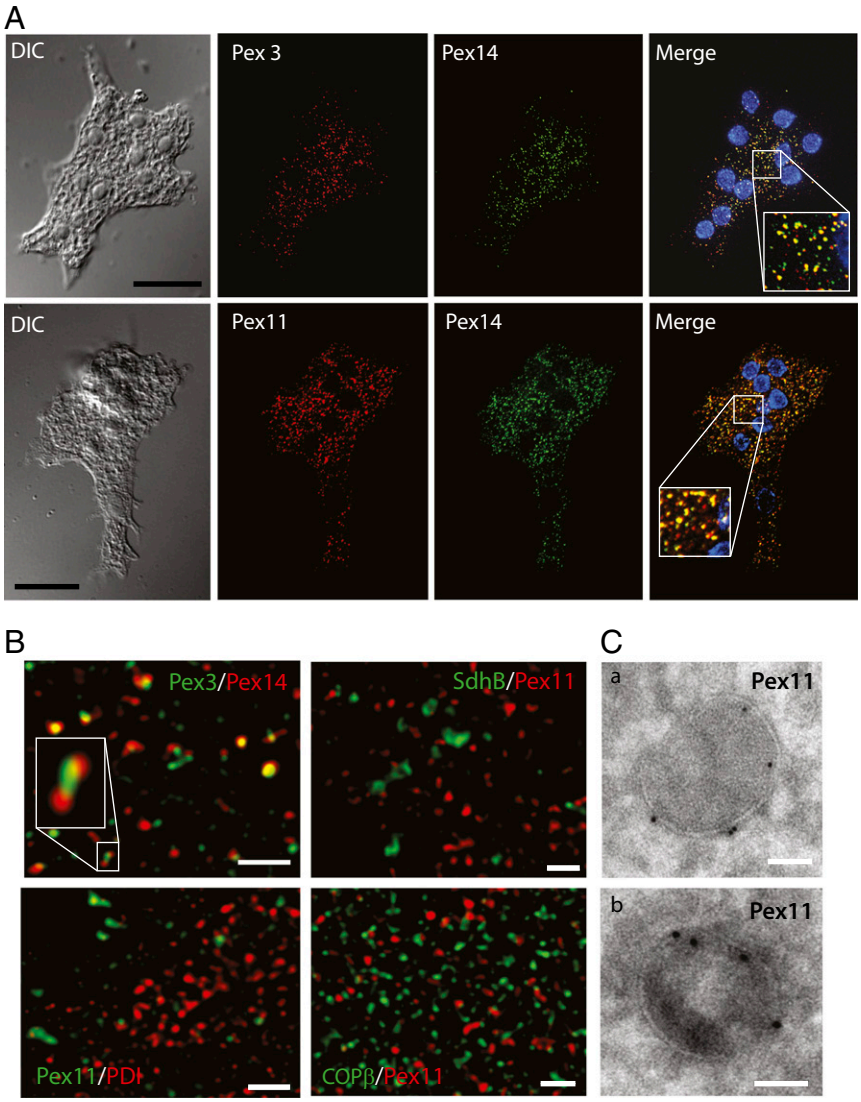

Fig. 2. Pexs colocalized in organelles distinct from hydrogenosomes, the Golgi apparatus, and the ER. (*A*) Confocal IF microscopy revealed colocalization of Pex3, Pex11-1, and Pex14. DIC, differential interference contrast. (Scale bar: 100 μm.) (*B*) STED microscopy analysis of Pex3, Pex11-1, Pex14, the hydrogenosomal marker succinate dehydrogenase (SdhB), the ER marker protein disulfide isomerase (PDI), and the Golgi marker COP β-subunit (COPβ), which were visualized using specific rat or rabbit polyclonal Abs. (Scale bar: 500 nm.) (*C*) Immunoelectron microscopy detection of Pex11-1 on *M. balamuthi* cryosections (*a* and *b*) using a polyclonal anti-Pex11-1 Ab and protein A conjugated with 5 nm gold particles. (Scale bar: 50 nm.)

that Pex11-1 is associated with a single membrane that surrounds vesicles with a dark matrix (Fig. 2*C* and *SI Appendix*, Fig. S4). The average size of these vesicles was 143 ± 38 nm (mean ± SD, $n = 20$) in diameter, which is within the range of sizes estimated by STED analysis. The number of putative peroxisomes in *M. balamuthi* was counted with Pex14 as a marker using confocal IF. We found 60 ± 20 peroxisomes per 100 μm^2 (mean ± SD, $n = 20$), which is comparable to the 50 to 119 glycosomes per 100 μm^2 determined in *Trypanosoma brucei* (30, 31) but higher than the 15.6 peroxisomes per 100 μm^2 found in human fibroblasts (32).

Finally, we selected *Mb*Pex14 to experimentally test its ability to target peroxisomes. Because *M. balamuthi* is not amenable to transformation, we used the yeast strain BY4742:POX1-EGFP expressing the integrated GFP-tagged peroxisomal marker protein acyl-CoA oxidase (Pox1), and this strain was transformed with a plasmid that allowed expression of *Mb*Pex14 fused with the fluorescent protein mCherry. Fluorescence microscopy of transformed cells cultivated with oleate to stimulate peroxisome formation showed that *Mb*Pex14 was incorporated into the Pox1-labeled peroxisomes. Western blot analysis of cellular fractions revealed that the majority of *Mb*Pex14 and Pox1 was present in the large granule fraction (LGF) (Fig. 3).

Matrix Proteins of *M. balamuthi* Peroxisomes. To identify the matrix components of the *M. balamuthi* peroxisomes, we initially searched for proteins with predicted PTS1 and PTS2 signals in the *M. balamuthi* genome. These searches revealed 664 proteins that possessed the predicted C-terminal PTS1 motif and 103 proteins with a putative PTS2 motif located within 100 amino acids (aa) of the N-terminal domain (Dataset S1). Next, we performed quantitative proteomic analysis of *M. balamuthi* subcellular fractions using the localization of organelle proteins by isotope tagging (LOPIT) method (33). Altogether, we identified 2,437 proteins in all fractions (Dataset S1). The distribution of peroxisomal proteins was traced using 5 membrane Pexs (*Mb*Pex3, *Mb*Pex10, *Mb*Pex11-1, *Mb*Pex12, and *Mb*Pex14) (Fig. 4). The peroxisomal markers had a higher relative abundance in fractions distinct from the marker proteins for hydrogenosomes and the ER (*SI Appendix*, Fig. S5 and Dataset S1). Next, we searched for proteins with quantitative distributions in cellular fractions similar to those determined for marker Pexs, which allowed the identification of 1,119 proteins, including additional Pexs: *Mb*Pex2, *Mb*Pex5, *Mb*Pex11-1, *Mb*Pex13, and *Mb*Pex16. Of these 1,119 proteins, 57 proteins contained a predicted PTS1/PTS2 motif (Fig. 4 and Dataset S1). Then, we removed 6 ribosomal proteins that are unlikely to reside in peroxisomes. The final dataset (*SI Appendix*, Table S3) contained 51 putative peroxisomal matrix proteins, of which 12 candidates were selected to validate their cell localization in yeast. Hydrogenosomal D-lactate dehydrogenase (D-LDH-M) and cytosolic NifU were used as controls for targeting specificity (18, 19). The proteins were expressed with an N-terminal mCherry tag in the yeast strain BY4742:POX1-EGFP. Fluorescence microscopy revealed that eight peroxisomal candidates (D-LDH; pantetheine-phosphate adenylyltransferase, PPAT; nudix hydrolase, Nudt; peroxisomal processing peptidase, PPP; inorganic pyrophosphatase 2, IPP-2; inositol dehydrogenase, IDH; tagatose-6-phosphate kinase, T6PK; and fumarylacetoacetate hydrolase, FAH) and the Pox1 marker colocalized together in yeast peroxisomes (Fig. 5 and *SI Appendix*, Table S3). As expected, NifU was localized to the cytosol, and D-LDH-M was localized to mitochondria. To investigate whether putative matrix proteins were translocated into the peroxisomal matrix, we performed a protein protection assay using D-LDH and PPAT. *Mb*Pex14 was used as a membrane marker. Both matrix proteins were fully membrane protected upon the treatment of LGF with proteinase K, whereas *Mb*Pex14 was partially cleaved (*SI Appendix*, Fig. S6).

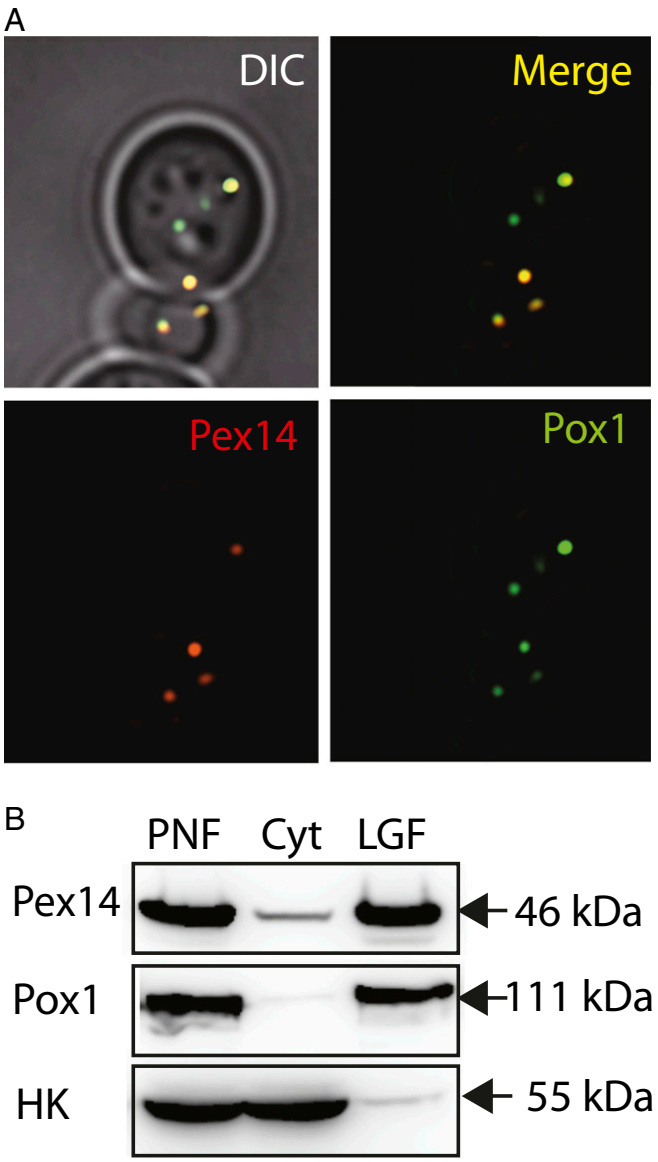

Fig. 3. *Mb*Pex14 is incorporated into *S. cerevisiae* peroxisomes. (*A*) Fluorescence microscopy of yeast expressing GFP-tagged Pox1 (peroxisomal marker) and mCherry-tagged Pex14 of *M. balamuthi*. DIC, differential interference contrast. Cells visualized at 1000× magnification. (*B*) Western blot analysis of the yeast postnuclear fraction (PNF), cytosol (Cyt), and large granule fraction (LGF). HK, hexokinase (cytosolic marker).

Although the ability of the tested *M. balamuthi* proteins to target yeast peroxisomes strongly supports their peroxisomal localization in *M. balamuthi*, we developed a specific polyclonal Ab against IPP-2 for its direct localization in *M. balamuthi*. IPP is particularly interesting because there are multiple paralogs of this enzyme with either N-terminal mitochondrial targeting sequences (IPP-1) (18) or a predicted C-terminal PTS1 (IPP-2, IPP-3, and IPP-4) (*SI Appendix*, Fig. S7). STED microscopy revealed that IPP-2 clearly colocalizes with Pex11-1–labeled vesicles (PCC $r = 0.53$). IPP-2 labeled smaller mostly round structures surrounded by the Pex11-1 signal (Fig. 6*A*). Elongated structures labeled with Pex11-1 were often associated with two separate blobs of IPP-2, which likely represent dividing peroxisomes. Immunoelectron microscopy revealed the presence of IPP-2 in the matrix of vesicles with a morphology similar to those in which we detected Pex11-1 (Figs. 2*C* and 6*B* and *SI Appendix*, Fig. S8). In double-labeling experiments,

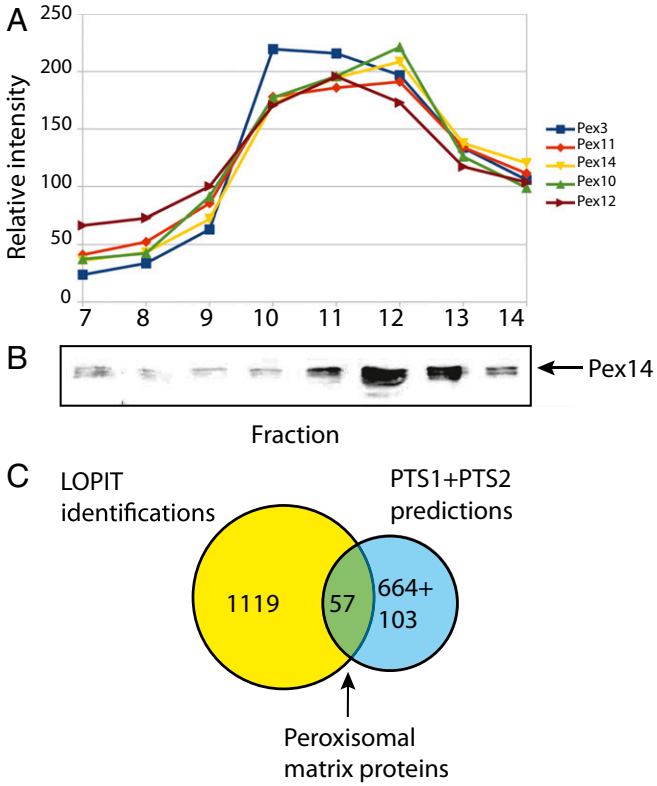

Fig. 4. Prediction of peroxisomal proteins using LOPIT and PTS1/PTS2 predictions. (*A*) Relative TMT intensities for marker Pexs in cellular fractions 7 to 14. (*B*) Western blot analysis of fractions 7 to 14 using an anti-Pex14 Ab. (*C*) Venn diagram depicting the intersection between the proteins identified by LOPIT and the proteins with a predicted PTS1/PTS2. Relative TMT intensities for hydrogenosomal and ER proteins are given in *SI Appendix*, Fig. S3.

both IPP-2 and Pex11-1 were observed in the matrix and at the membrane, respectively, within the same organelle (Fig. 6*C*).

Next, we tested whether the targeting of selected *M. balamuthi* candidates to peroxisomes was dependent on the predicted PTS1 signal. The proteins were expressed in BY4742:POX1-EGFP yeast with or without PTS1, and their presence was traced in the cytosolic fraction and LGF by Western blot. All proteins with truncated C-termini were significantly reduced or absent in the LGF (Fig. 7). The PTS1 motif of proteins that were successfully targeted to peroxisomes included two proteins (Nudt and PPP) with the classic C-terminal SKL tripeptide, whereas other proteins possessed its variants, which included ARL (D-LDH), AKL (IPP-2, IDH, and PPAT), SRL (T6PK), and ARM (FAH). Based on these experiments, the PTS1 consensus sequence of *M. balamuthi* peroxisomal proteins appeared to be [S/A][R/K][L/M], which corresponds well to the broader consensus sequence [S/A/P/C][K/R/H][L/M/I] established for peroxisomes of metazoans, plants, and glycosomes of kinetoplastids (34, 35).

The identification of PPP among peroxisomal proteins of *M. balamuthi* is noteworthy, as it is believed that PPP is present only in multicellular organisms (36). Our homology searches in available genomes of amoebozoans revealed the presence of PPP orthologs in mycetozoans such as *D. discoideum* and in *Acanthamoeba castellanii*; however, we did not find PPP in entamoebids (*SI Appendix*, Fig. S9). PPP was also detected in selected members of the eukaryotic supergroups SAR and Excavata. In the latter group, PPP was found in *Naegleria*, but it was absent in kinetoplastid glycosomes. Phylogenetic analysis revealed a monophyletic origin of PPPs, including *M. balamuthi*, other unicellular eukaryotes, and the known PPPs Tysnd1

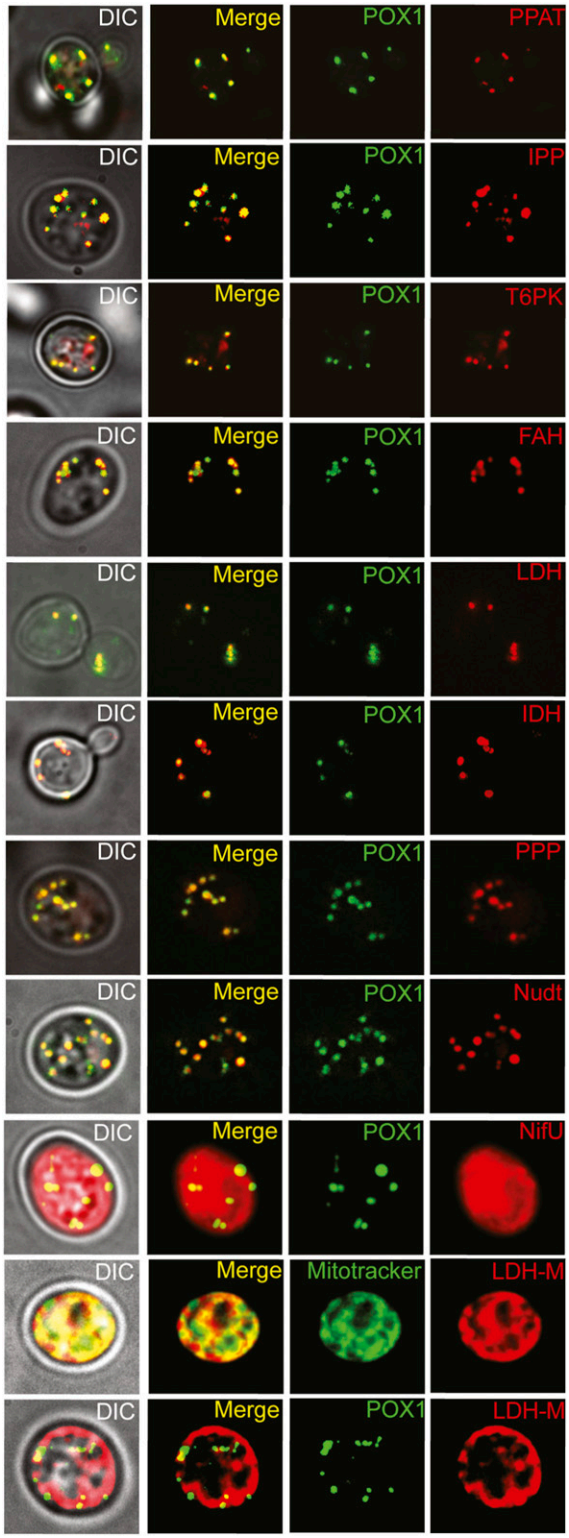

Fig. 5. Localization of *M. balamuthi* peroxisomal matrix candidates in *S. cerevisiae* peroxisomes. GFP-tagged Pox1 was used as a peroxisomal marker. mCherry-tagged *M. balamuthi* proteins: FAH, fumarylacetoacetate hydrolase; IPP, inorganic pyrophosphatase 2; Nudt, nudix hydrolase; T6PK, tagatose-6-phosphate kinase; LDH, lactate dehydrogenase; PPAT, pantetheine-phosphate adenylyltransferase; IDH, inositol dehydrogenase; PPP, peroxisomal processing peptidase; NifU, cytosolic marker; and LDH-M, hydrogenosomal paralog of lactate dehydrogenase. DIC, differential interference contrast. Cells visualized at 1000× magnification.

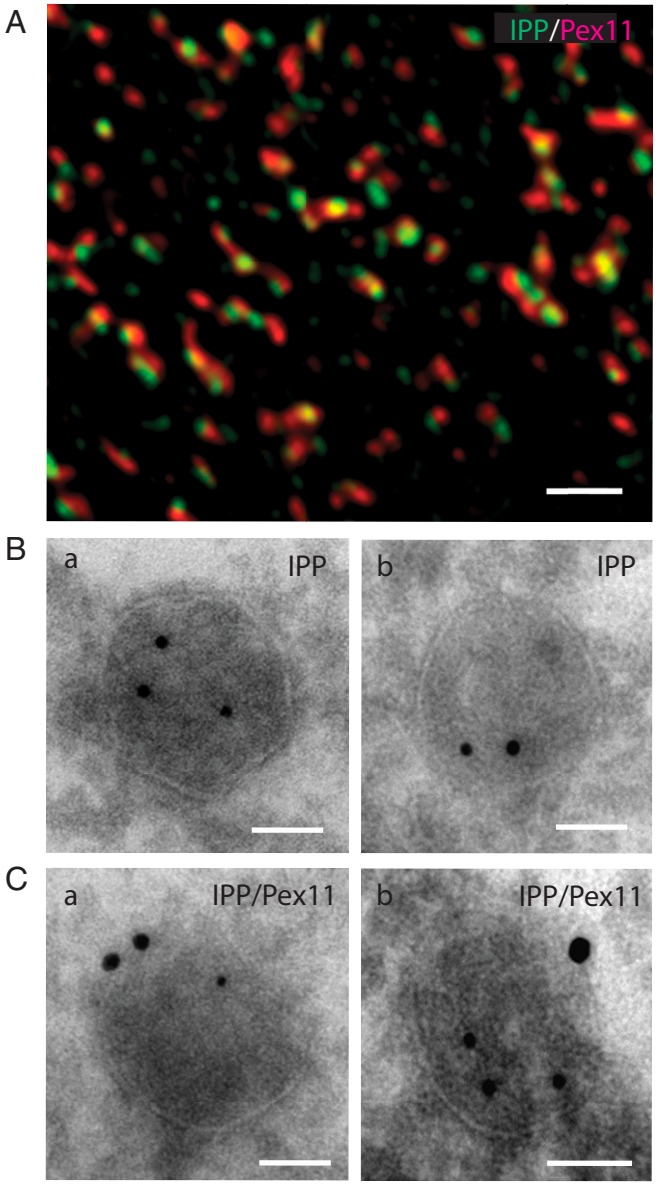

Fig. 6. Immunolocalization of the peroxisomal matrix protein IPP-2 in *M. balamuthi*. (*A*) STED microscopy using specific polyclonal Abs against IPP-2 (green) and Pex11-1 (red). (Scale bar: 500 nm.) (*B*) Immunoelectron microscopy detection of IPP-2 on *M. balamuthi* cryosections (*a* and *b*) using a rat polyclonal anti–IPP-2 Ab and anti-rat IgG conjugated with 10 nm gold particles. (*C*) Colocalization of IPP-2 and Pex11 (*a* and *b*). IPP-2 was detected using a rat polyclonal anti–IPP-2 Ab and anti-rat IgG conjugated to 10 nm gold particles, Pex11-1 was detected using a rabbit polyclonal anti–Pex11-1 Ab with secondary anti-rabbit IgG conjugated with 15 nm gold particles. (Scale bar: 50 nm.)

and Deg15 in metazoans and plants, respectively, that formed group IV (*SI Appendix*, Fig. S9). All members of this group possessed PTS1, mostly with the SKL tripeptide, including the *M. balamuthi* PPP.

Predicted Metabolic Pathways. Neither bioinformatic nor proteomic analyses identified any component of typical peroxisomal pathways associated with oxygen metabolism, such as β-oxidation or catalase (Dataset S1 and *SI Appendix*, Table S4). However, we identified components of acetyl-CoA metabolism, pyrimidine biosynthesis, and carbohydrate metabolism (Fig. 8 and *SI Appendix*, Table S4). PPAT is a candidate that is potentially involved in the regulation of peroxisomal CoA levels. This enzyme catalyzes the second-to-last step in CoA synthesis (Fig. 8 and *SI Appendix*, Fig. S10). The following step of CoA synthesis is catalyzed by

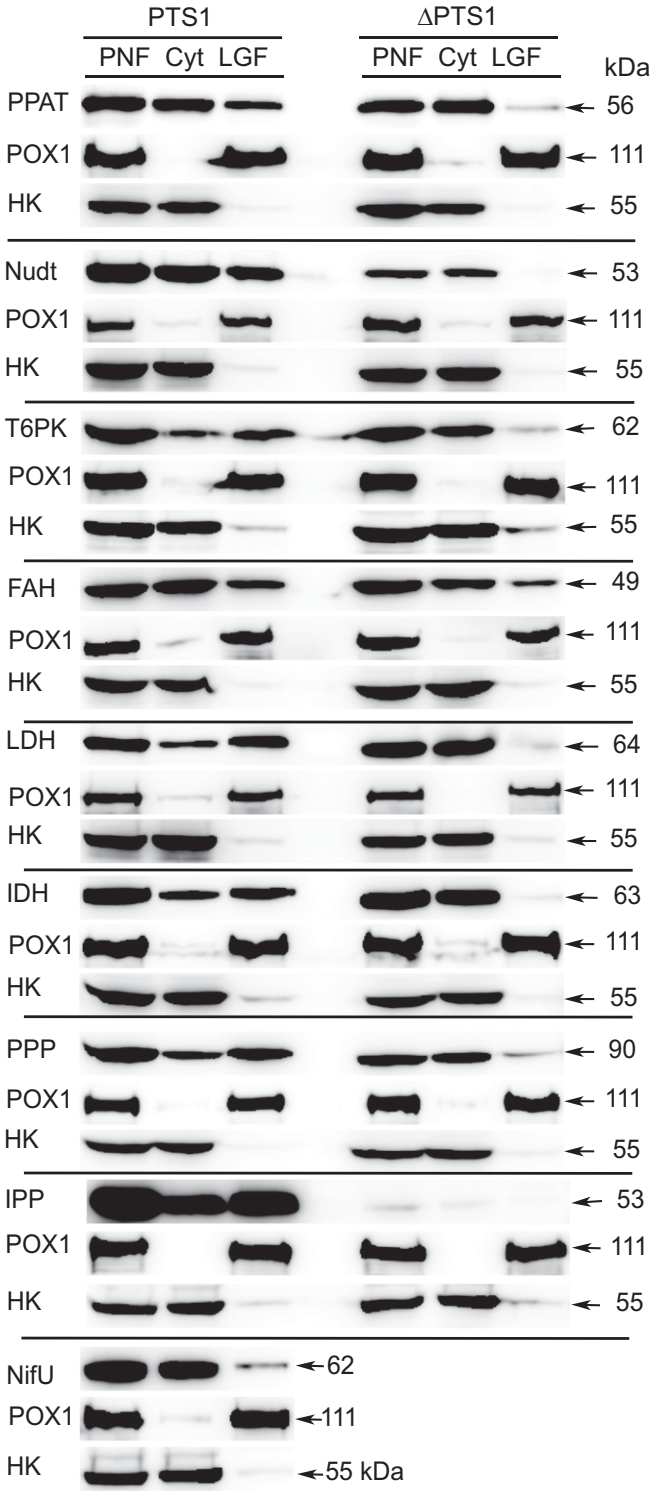

Fig. 7. PTS1-dependent import of *M. balamuthi* proteins into *S. cerevisiae* peroxisomes. *M. balamuthi* peroxisomal matrix proteins with the PTS1 signal or without the 13 C-terminal aa (ΔPTS1) were expressed in yeast. *M. balamuthi* proteins were detected using an anti-mCherry Ab, Pox1 was detected with an anti-GFP Ab, and hexokinase (HK) was used as a cytosolic marker and detected using anti-*S. cerevisiae* HK Ab.

dephospho-CoA kinase (DPCK), which is encoded in the genome (m51a1_g647); however, DPCK was not identified in the proteome. CoA and ATP are required for the activation of fatty acids by acyl-CoA synthetase (ACS). We identified two ACS paralogs with LOPIT support; however, only ACS-1 possessed a predicted PTS1 motif (*SI Appendix*, Fig. S11) (37). ACS is linked with IPP, which cleaves PPi to prevent the reverse reaction. Indeed, we identified two IPP paralogs (IPP-2 and IPP-3) in *M. balamuthi* peroxisomes (*SI Appendix*, Table S3). Pyrimidine biosynthesis includes the conversion of dihydroorotate to uridylate. This pathway requires the activities of three enzymes: dihydroorotate dehydrogenase (DHODH), orotate phosphoribosyl transferase (OPRT), and orotidine-5′-monophosphate decarboxylase (OMPD). In the *M. balamuthi* genome, we identified a single gene encoding a fused protein with PTS1 (ANL), which contains domains for all three enzymes, including an N-terminal DHODH domain, followed by OPRT and OMPDC (*SI Appendix*, Fig. S12). OPRT and OMPDC are often fused in eukaryotes to form a single peroxisomal protein, whereas DHODH functions as a separate protein, either in the cytosol (bacterial class 1) or in mitochondria (class 2) (38) (*SI Appendix*, Fig. S12). Therefore, we performed phylogenetic analysis of the *M. balamuthi* OMPDC-OPRT-DHODH domains. All three components appeared to be of bacterial origin, including DHODH, which clustered with class 1A orthologs present in bacteria, kinetoplastids, and diatoms (*SI Appendix*, Fig. S13 *A–C*). The activity of DHODH class 1A is dependent on fumarate as an electron acceptor that could be produced in *M. balamuthi* by peroxisomal FAH or imported from the cytosol, where fumarate is formed by fumarase, which is encoded in the *M. balamuthi* genome (m51a1_g4783) (Fig. 8). OPRT activity required 5-phosphoribosyl-1-pyrophosphate (PRPP), which is formed from D-ribose phosphate by the activity of ribose-5-phosphate diphosphokinase. We predicted two alternative pathways for the formation of D-ribose phosphate via either glucose-6-phosphate dehydrogenase or the ADP ribose diphosphatase activity of Nudt. However, nudix hydrolases represent a large protein family with various functions, and the protein sequence analysis of *Mb*Nudt did not allow us to unequivocally predict its substrate specificity (*SI Appendix*, Fig. S14). Carbohydrate metabolism includes the putative D-LDH, IDH, and T6PK with a PTS1 and malate dehydrogenase (MDH) with a PTS2 (Fig. 8 and *SI Appendix*, Table S3 and Figs. S15 and S16). Altogether, these results indicate the presence of peroxisomes in the anaerobic protist *M. balamuthi*.

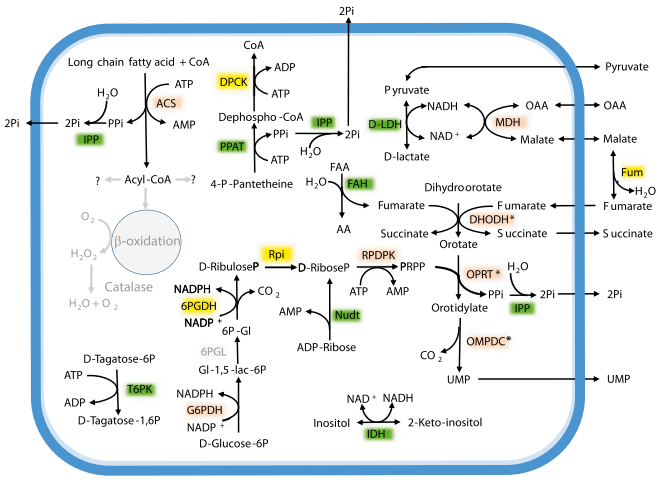

Fig. 8. Predicted metabolism of *M. balamuthi* anaerobic peroxisomes. The green box indicates enzymes that were localized in yeast peroxisomes; the pink box indicates proteins with a predicted PTS1/2 and support for peroxisomal localization by LOPIT (*SI Appendix*, Table S5); the yellow box indicates genes identified in the *M. balamuthi* genome; and gray indicates enzymes: ACS, Acyl-CoA synthetase; DPCK, dephospho-CoA kinase; FAH, fumarylacetoacetate hydrolase; Fum, fumarase; G6PDH, glucose-6-phosphate dehydrogenase; IDH, inositol dehydrogenase; IPP, inorganic pyrophosphatase; 6PGDH, 6-phosphogluconate dehydrogenase; DHODH, dihydroorotate dehydrogenase; OPRT, orotate phosphoribosyl transferase; OMPDC, orotidine-5′-monophosphate decarboxylase; MDH, malate dehydrogenase; Nudt, nudix hydrolase; 6-phosphogluconolactonase, 6PGL; 6-phosphogluconate dehydrogenase, 6PGDH; PPAT, pantetheine-phosphate adenylyltransferase; RPDPK, ribose-5- phosphate diphosphokinase; ribose phosphate isomerase, Rpi; and T6PK, tagatose-6-phosphate kinase. Substrates are as follows: AA, acetoacetate; FAA, fumarylacetoacetate; PRPP, 5-phosphoribosyl-1-pyrophosphate; Gl-1,5-lac-6P, D-glucono-1,5-lactone-6-phosphate; D-glucose-6P; OAA, oxalacetate; D-tagatose-6P, D-tagatose-6-phosphate; D-tagatose-1,6-bisphosphate; D-riboseP, D-ribose phosphate; and PPi, pyrophosphate. *Domains of the fusion enzyme DHODH-OPRT-OMPDC.

Discussion

Free-living *M. balamuthi* is a eukaryote characterized as possessing both an anaerobic type mitochondria (hydrogenosomes) and peroxisomes. These "anaerobic" peroxisomes lack metabolic pathways generating ROS, such as β-oxidation, as well as ROS-detoxifying enzymes, including catalase. However, they contain components of acyl-CoA and carbohydrate metabolism and pyrimidine and CoA biosynthesis. *M. balamuthi* possesses a set of 14 Pexs required for the biogenesis of peroxisomes and machinery for the targeting of proteins to the peroxisome via PTS1/PTS2 and PPP.

In other eukaryotes with anaerobic forms of mitochondria, peroxisomes are believed to be absent (15, 16). Two proteins (ACS and Pex-4) were recently suggested to represent putative peroxisomal remnants in *Giardia intestinalis*, but their significance needs to be clarified (39). In addition to anaerobes, the absence of peroxisomes was noted in parasitic organisms with unconventional mitochondria such as *Plasmodium falciparum* and related species of the Aconoidasida group that live in aerobic niches (40, 41). However, during erythrocytic stages, *Plasmodium* relies mainly on cytosolic glycolysis, similar to anaerobes. In addition, the absence of peroxisomes has been predicted in several lineages of parasitic helminths (42), most of which adapted to oxygen-poor environments and can gradually replace the TCA cycle and aerobic phosphorylation with anaerobic energy metabolism (43). The identification of peroxisomes in anaerobic *M. balamuthi* is thus unprecedented, considering the correlation between the adaptation of mitochondria to anaerobiosis and the loss of peroxisomes.

Four peroxisomal proteins, Pex3, Pex10, Pex12, and Pex19, which are considered unequivocal in silico peroxisomal markers (2), and 10 other Pexs (Pex1, Pex2, Pex5, Pex6, Pex7, Pex11-1, Pex11-2, Pex13, Pex14, and Pex16), were identified in the *M. balamuthi* genome. Ten of 14 predicted Pexs were identified by proteomics, which indicates that these proteins are available for peroxisome biogenesis. Targeting of *M. balamuthi* matrix proteins with PTS1 to peroxisomes was experimentally confirmed in *S. cerevisiae*. Notably, *M. balamuthi* peroxisomes seem to retain the PTS2 system, which is not as universally distributed as PTS1 (42, 44–46). As in other peroxisome-bearing organisms, ubiquitination-dependent recycling of PTS receptors likely occurs in anaerobic peroxisomes with contributions from the Pex2/10/12 RING-finger complex and the AAA-type ATPases Pex1/6. Although we did not identify a Pex4 ortholog in *M. balamuthi*, Pex4 could be functionally replaced by other enzymes with the required activity. For example, in humans, Pex4 is functionally replaced by the related ubiquitin-conjugating proteins Ubc5a/b/c (47). *M. balamuthi* possesses all three members of the machinery that target proteins to the peroxisomal membrane, *Mb*Pex3, *Mb*Pex16, and *Mb*Pex19. Pex19 is a soluble shuttling receptor that was not found in the LOPIT data; however, a single gene encoding a putative *Mb*Pex19 was found in the *M. balamuthi*

genome. Finally, *M. balamuthi* possesses two *Mb*Pex11 paralogs that may facilitate the elongation of the peroxisomal membrane and the fission of the organelles (23, 24). Collectively, these findings show that *M. balamuthi* anaerobic peroxisomes contain a rather standard set of Pexs that are required for peroxisome biogenesis.

In contrast, most typical peroxisomal metabolic pathways, such as β-oxidation and hydrogen peroxide detoxification, are absent or highly reduced in *M. balamuthi*. We predicted the presence of ACS, which requires CoA as an obligate cofactor for the activation of medium- and long-chain fatty acids. This enzyme activates the substrate mainly for β-oxidation (37); however, because β-oxidation is absent in *M. balamuthi* and we did not find any other acyl-CoA–dependent degradation or biosynthetic pathways, the fate of acyl-CoA in anaerobic peroxisomes is currently unknown. Interestingly, anaerobic peroxisomes are likely involved in CoA synthesis via the PPAT and DPCK pathways. This is supported by intraperoxisomal localization of *Mb*PPAT, which was predicted by LOPIT data and demonstrated by the protein protection assay, although the cell localization of DPCK in *M. balamuthi* remains unclear. In most eukaryotes, CoA synthesis is compartmentalized to the cytosol or plastids, and in mammalian cells, PPAT and DPCK form the fusion protein CoA synthase that is partially associated with the mitochondrial outer membrane (48, 49). The peroxisomal localization of CoA synthesis has not been reported thus far, although DPCK has been found in the *Arabidopsis* peroxisomal proteome (50).

There are several enzymes that could be involved in the maintenance of the redox balance of anaerobic peroxisomes. We can predict that MDH serves as a redox shuttle enzyme that oxidizes NADH, whereas the metabolites oxaloacetate and malate cross the peroxisomal membrane as they do in plant peroxisomes (51). In addition, there are two more enzymes that are known to mediate peroxisomal redox balance, NAD-dependent D-LDH and NADP-dependent glucose-6-phosphate dehydrogenase (G6PDH). D-lactate and malate exported from peroxisomes can be taken up by hydrogenosomes as substrates for hydrogenosomal D-LDH and MDH, respectively (18). G6PDH is an enzyme of the pentose phosphate pathway, which operates in the cytosol; however part of this pathway involving G6PDH was found in peroxisomes and glycosomes (52, 53).

Our data suggest that anaerobic peroxisomes possess a significant part of the de novo pyrimidine synthesis pathway. We found a unique fusion protein with three OMPDC-OPRT-DHODH domains that may convert dihydroorotate to uridylate. The DHODH domain corresponds to class 1A DHODH, which is typically a bacterial protein and is critical for the synthesis of pyrimidine under anaerobiosis using fumarate as an electron acceptor (54, 55). Most eukaryotes, including the aerobic amoeba *D. discoideum*, possess mitochondrial DHODH class 2 that provides electrons to ubiquinone (56, 57). Thus, the acquisition of class 1A DHODH by *M. balamuthi* is likely associated with the adaptation of this lineage to anaerobiosis. DHODH is known as a cytosolic or mitochondrial protein, whereas the next two steps converting orotate to uridylate (UMP) via the activities of OPRT and OMDC take place in peroxisomes or glycosomes (58). Interestingly, various combinations of OPRT and OMDC have been reported in fusion proteins from eukaryotes and bacteria (59). However, none of the known fusion proteins are fused with DHODH, as found in *M. balamuthi*, which may allow the conversion of dihydroorotate to uridylate in a single compartment.

Surprisingly, *M. balamuthi* peroxisomes contain a putative T6PK. This finding is supported by the LOPIT data, the presence of PTS1, and targeting to yeast peroxisomes. T6PK belongs to the ATP-dependent phosphosugar kinase (PfkB) family of mainly bacterial enzymes (60). In eukaryotes, T6PK was predicted to reside in the glycosome of *Leishmania major* (61), and genes for T6PK are annotated in genomes of other *Leishmania* species, leptomonads and *Entamoeba* species.

Is there any relationship between anaerobic peroxisomes and hydrogenosomes? Analysis of peroxisomal matrix proteins revealed the presence of at least three enzymes (MDH, D-LDH, and IPP) with dual localization in peroxisomes and hydrogenosomes. Each enzyme seems to employ different mechanisms for dual protein targeting. Gene duplication and acquisition of different targeting signals are involved in the dual localization of D-LDH. It has been shown that *M. balamuthi* possesses two closely related copies of D-LDH (18). The first copy, D-LDH-M, is targeted to hydrogenosomes via N-terminal targeting sequence (NTS) (18). Here, we found that the second D-LDH copy possesses a C-terminal extension with a PTS1 signal, whereas the NTS is absent. When D-LDH was expressed with an N-terminal tag in yeast, the protein appeared in peroxisomes (this study), whereas previous localization of this D-LDH with a C-terminal tag that masked PTS1 resulted in cytosolic mislocalization (18). IPP is present in four copies (this work and ref. 18). IPP-1 is targeted to hydrogenosomes via NTS, whereas IPP-2, IPP-3, and IPP-4 possess PTS1. However, in contrast to D-LDH paralogs, the origin of hydrogenosomal and peroxisomal IPPs is different (18). IPP-1 is eukaryotic in origin and clusters together with the mitosomal IPP in *Entamoeba histolytica*, whereas IPP-2 and -3 were most likely acquired by lateral gene transfer (LGT) from bacteria (18). Bioinformatic analysis of MDH predicted multiple signals within the N-terminal extension. There are three nearly identical copies with a hydrogenosomal NTS and a cleavage site for mitochondrial processing peptidase between the amino acid residues at positions 30 to 31 (18, 62). Peroxisomal localization of MDH is most likely driven by PTS2, which has been predicted at positions 11 to 19 within the NTS. Similar cotargeting to peroxisomes and mitochondria mediated by the bifunctional N-terminal domain was observed for the yeast catalase Cta1p (63).

The discovery of anaerobic peroxisomes in *M. balamuthi* provides a perspective for studies of the evolution of eukaryotes that live in the absence of oxygen. In the last two decades, great progress has been made in this direction. However, most studies have focused on investigations of anaerobic forms of mitochondria. Genomic and transcriptomic analyses of parasitic, endosymbiotic, and free-living protists revealed a functional continuum from strictly oxygen-dependent mitochondria via mitochondria of facultatively anaerobic organisms adapted to an anaerobic lifestyle to various extents to highly reduced mitosomes in parasitic species (64, 65). In contrast, peroxisomes were considered to be present in aerobes and absent in anaerobes based on few examples of anaerobic protists, such as *Trichomonas vaginalis*, *G. intestinalis*, and *E. histolytica*, in which peroxisomes have not been found (2, 66, 67). The discovery of peroxisomes in anaerobic *M. balamuthi* with hydrogenosomes and anaerobic energy metabolism may change this view and turn attention to the evolution of peroxisomes in anaerobic or facultatively anaerobic organisms. In particular, it would be interesting to investigate how peroxisomes and mitochondria coevolved, reflecting the presence of oxygen in the environment and reconsidering the role of oxygen and ROS in the evolution of peroxisomes.

Materials and Methods

Cell Cultivation. *M. balamuthi* (ATCC 30984) was maintained axenically in proteose peptone–yeast extract–glucose–cysteine (PYGC) medium at 24 °C (68). The *S. cerevisiae* strain BY4742:POX1-EGFP (69) was grown in a rich or selective medium as previously described (70). The formation of peroxisomes was stimulated using oleate medium containing 0.05% yeast extract and 0.1% oleic acid (71).

Bioinformatics. Genes encoding *M. balamuthi* Pexs were obtained by TBLAST searches of the draft *M. balamuthi* genome sequence available at the Orcae database (https://bioinformatics.psb.ugent.be/orcae/, refs. 19 and 72) using the orthologous sequences of *S. cerevisiae*. Searches for PTS1 in 14,841 predicted

proteins of *M. balamuthi* given in *SI Appendix*, Table S3 were performed using PeroxisomeDB (http://www.peroxisomedb.org/) considering 12 C-terminal residues (73). PTS2 was locally predicted using the consensus sequence (R/K)-(L/I/V)-X5-(H/Q)-(L/A) (50, 74, 75). Transmembrane domains were predicted using TMHMM server v2.0 (http://www.cbs.dtu.dk/services/TMHMM/). Predicted peroxisomal proteins were annotated using the eggNOG database (http://eggnogdb.embl.de/).

Protein Expression and Antibodies. Recombinant *M. balamuthi* Pex14 and IPP-2 were produced in *Escherichia coli* BL21 Rosetta cells (Novagen) using the pET42b expression vector (Novagen). Partial sequences of Pex3 and Pex11-1 were produced using pETM11-SUMO2-GFP (76). Abs against Pex3, Pex11-1, Pex14, and IPP-2 were raised in rats and rabbits (Davids Biotechnologie GmbH). The other Abs included a rat polyclonal anti-PDI Ab (29), rat polyclonal anti-COPI β-subunit Ab (29), rat polyclonal anti-succinate dehydrogenase (Sdh) β-subunit Ab (19), rabbit polyclonal anti-hexokinase Ab (a kind gift from Doron Rapaport, University of Tübingen, Tübingen, Germany), and mouse monoclonal anti-GFP Ab (Santa Cruz Biotechnology, Inc.). Details of gene cloning and protein expression are given in *SI Appendix, Materials and Methods*.

Expression and Localization of Proteins in *S. cerevisiae*. Genes for *M. balamuthi* peroxisomal candidates were amplified and subcloned (*SI Appendix, Materials and Methods* and Table S5) into a modified pTVU100 vector (77) that allows protein expression in yeast with an N-terminal mCherry tag (pTVU100-N-mCherry). *S. cerevisiae* BY4742:POX1-EGFP (kindly provided by Zdena Palková, Charles University, Prague, Czech Republic) was transformed with the pVTU constructs using the lithium acetate/single-stranded carrier DNA/PEG method (78). Transformed strains were selected and maintained on uracil-free medium. Cells were incubated for 15 to 20 h in oleate medium prior to microscopy. For the investigation of PTS1-dependent protein targeting to yeast peroxisomes, the genes of interest were subcloned into the same vector without sequences coding for the 13 aa at the C-terminus.

Light Microscopy. For IF, *M. balamuthi* cells were processed as described (18). Images were obtained with a Leica SP8 confocal laser scanning microscope (Leica Microsystems). Images were deconvolved with Huygens Professional version 17.10 (Scientific Volume Imaging, The Netherlands, https://svi.nl/HomePage) and further processed using Fiji software (79). PCC was calculated using JACoP (80). The peroxisome number was determined in *M. balamuthi* cells using Pex14 as a marker. The number of labeled organelles and the corresponding cell area were determined per 20 cells using Icy software (81). To compensate for large variations in cell size, the number of peroxisomes was expressed per 100 μm^2.

To observe GFP- and mCherry-tagged proteins in *S. cerevisiae* transformants, living yeast in synthetic medium were immobilized in 0.2% agarose on slides. Fluorescence signals of GFP, mCherry, and 4′,6-diamidino-2-phenylindole (DAPI) were detected using a Nikon Eclipse TiE with an Andor iXon Ultra DU897 camera (Nikon Instruments, Inc.) and processed as described above.

STED microscopy was performed as described previously (82). Images were obtained using an Abberior STED 775 QUAD scanning microscope (Abberior Instruments GmbH) equipped with a Nikon CFI Plan Apo Lambda objective and deconvolved with Huygens Professional version software 17.04 using the classic maximum likelihood estimation algorithm. The secondary Abs were Abberior STAR 580 anti-rat or rabbit Abs and Abberior STAR 635p anti-rat or anti-rabbit Abs.

Transmission Immunoelectron Microscopy. Immunogold labeling of thawed cryosections (Tokuyasu technique) was used to detect Pex11-1 and IPP-2 as described (*SI Appendix, Materials and Methods*) (83). The sections were incubated for 30 min at room temperature with a rabbit polyclonal anti-PEX11-1 Ab, a polyclonal rat IPP-2 Ab, or a mixture of both Abs. For detection, we used various secondary probes conjugated to gold nanoparticles of different sizes: protein A conjugated with 5 nm nanoparticles (University Medical Centre, Utrecht, The Netherlands), goat anti-rabbit IgG-15 nm (BBI Solutions), and goat anti-rat IgG conjugated with 10 nm nanoparticles (BBI Solutions). The samples were observed using a JEOL 1010 transmission electron microscope.

Fractionation of *M. balamuthi* Cells. Subcellular fractions of *Mastigamoeba* were obtained by differential and Percoll gradient centrifugation of the cell homogenate. Fifteen fractions (0.5 mL each) were collected, washed, and analyzed by Western blot using Ab against Pex14. Eight fractions with a Pex14 signal were submitted for quantitative mass spectrometry. Details of cellular fractionation are given in *SI Appendix, Materials and Methods*.

Isolation of the LGF from *S. cerevisiae*. The yeast LGF was obtained using previously described methods (84) with modifications given in *SI Appendix, Materials and Methods*.

LOPIT. Protein samples (50 μg) were processed and trypsin digested as described previously (85). Tandem mass tag (TMT) reagents were added to each sample according to the manufacturer's protocol (Thermo Scientific Pierce), and after 60 min, the reaction was stopped by the addition of 0.5% hydroxylamine. Peptides were separated using a C18 column (Kinetex 1.7 μm, EVO C18, 150 × 2.1 mm). Thirty-four fractions were collected, and each of the 2 most distant fractions was pooled into 17 fractions as described previously (86). Data acquisition was performed as described previously using a Thermo Orbitrap Fusion (Q-OT- qIT, Thermo Fisher Scientific) (85).

Raw data were processed in Proteome Discoverer 2.1. (Thermo Fisher Scientific). Searches were performed against a local *M. balamuthi* protein database with 14,841 entries and a common contaminant database. To predict the cellular localization of peroxisomal proteins, marker proteins with the expected localization were used for the detection of fractions with maximum TMT values. The following markers were used—peroxisomes: Pex3, Pex10, Pex11, Pex12, and Pex14; hydrogenosomes: Tom40, voltage-dependent anion channel (VDAC), Cpn60, Cpn10, Sdh subunits A and C, ADP/ATP carrier, hydrogenosomal NifS, and T- and H-protein of the glycine cleavage system (Gcs); and ER: Sec61, Sec22, reticulon, signal recognition particle receptor subunit α (SRPRA), calnexin, and PDI. To filter putative peroxisomal matrix proteins, we used the following criteria: the protein was detected by more than one peptide in at least one of two independent fractionations with a maximum TMT value within the range of peroxisomal markers; it possesses predicted PTS1 or PTS2 consensus sequences; and it lacked predicted transmembrane domains. More details are given in *SI Appendix, Materials and Methods*.

Data Availability. MaxQuant results were uploaded to the PRIDE partner repository (https://www.ebi.ac.uk/pride/archive/) with the dataset identifier PXD014205. The sequences reported in this paper have been deposited in the online resource for community annotation of eukaryotes (ORCAE, https://bioinformatics.psb.ugent.be/orcae/) and are given in Dataset S1.

ACKNOWLEDGMENTS. This work was supported by the Czech Science Foundation (16-06123S), Národní Program Udržitelnosti II (LQ1604) provided by the Ministry of Education, Youth, and Sport of the Czech Republic, Project CePaViP (CZ.02.1.01/0.0/0.0/16_019/0000759), provided by European Regional Development Fund, and the MICOBION project funded by European Union H2020 (810224). T.L. was supported by Charles University Grant Agency 170218. We thank the Imaging Methods Core Facility at BIOCEV for STED microscopy; the Core Facility of the Institute of Parasitology and Biology Centre of the Czech Academy of Sciences (České Budějovice, Czech Republic) for electron microscopy, both supported by the Czech-BioImaging RI project LM2015062; the core facility OMICS Proteomics BIOCEV for MS analysis; and Michaela Marcinciková and Eliška Kočířová for technical assistance.

1. T. Gabaldón, Peroxisome diversity and evolution. *Philos. Trans. R. Soc. Lond. B Biol. Sci.* **365**, 765–773 (2010).
2. A. Schlüter *et al*., The evolutionary origin of peroxisomes: An ER-peroxisome connection. *Mol. Biol. Evol.* **23**, 838–845 (2006).
3. C. De Duve, P. Baudhuin, Peroxisomes (microbodies and related particles). *Physiol. Rev.* **46**, 323–357 (1966).
4. J. J. Smith, J. D. Aitchison, Peroxisomes take shape. *Nat. Rev. Mol. Cell Biol.* **14**, 803–817 (2013).
5. L. Pieuchot, G. Jedd, Peroxisome assembly and functional diversity in eukaryotic microorganisms. *Annu. Rev. Microbiol.* **66**, 237–263 (2012).
6. K. Bolte, S. A. Rensing, U. G. Maier, The evolution of eukaryotic cells from the perspective of peroxisomes: Phylogenetic analyses of peroxisomal beta-oxidation enzymes support mitochondria-first models of eukaryotic cell evolution. *BioEssays* **37**, 195–203 (2015).
7. D. Speijer, Evolution of peroxisomes illustrates symbiogenesis. *BioEssays* **39**, 1700050 (2017).
8. C. de Duve, The origin of eukaryotes: A reappraisal. *Nat. Rev. Genet.* **8**, 395–403 (2007).
9. T. Gabaldón, A metabolic scenario for the evolutionary origin of peroxisomes from the endomembranous system. *Cell. Mol. Life Sci.* **71**, 2373–2376 (2014).
10. T. Gabaldón, Evolutionary considerations on the origin of peroxisomes from the endoplasmic reticulum, and their relationships with mitochondria. *Cell. Mol. Life Sci.* **71**, 2379–2382 (2014).
11. M. Schrader, J. Costello, L. F. Godinho, M. Islinger, Peroxisome-mitochondria interplay and disease. *J. Inherit. Metab. Dis.* **38**, 681–702 (2015).
12. M. Fransen, M. Nordgren, B. Wang, O. Apanasets, Role of peroxisomes in ROS/RNS-metabolism: Implications for human disease. *Biochim. Biophys. Acta* **1822**, 1363–1373 (2012).

13. M. P. Menendez-Gutierrez, T. Roszer, M. Ricote, Biology and therapeutic applications of peroxisome proliferator- activated receptors. *Curr. Top. Med. Chem.* **12**, 548–584 (2012).
14. A. Sugiura, S. Mattie, J. Prudent, H. M. McBride, Newly born peroxisomes are a hybrid of mitochondrial and ER-derived pre-peroxisomes. *Nature* **542**, 251–254 (2017).
15. E. Gentekaki *et al*., Extreme genome diversity in the hyper-prevalent parasitic eukaryote Blastocystis. *PLoS Biol.* **15**, e2003769 (2017).
16. T. Gabaldón, M. L. Ginger, P. A. M. Michels, Peroxisomes in parasitic protists. *Mol. Biochem. Parasitol.* **209**, 35–45 (2016).
17. T. M. Embley, W. Martin, Eukaryotic evolution, changes and challenges. *Nature* **440**, 623–630 (2006).
18. E. Nývltová *et al*., Lateral gene transfer and gene duplication played a key role in the evolution of *Mastigamoeba balamuthi* hydrogenosomes. *Mol. Biol. Evol.* **32**, 1039–1055 (2015).
19. E. Nývltová *et al*., NIF-type iron-sulfur cluster assembly system is duplicated and distributed in the mitochondria and cytosol of *Mastigamoeba balamuthi*. *Proc. Natl. Acad. Sci. U.S.A.* **110**, 7371–7376 (2013).
20. H. Hayashi, T. Suga, Some characteristics of peroxisomes in the slime mold, Dictyostelium discoideum. *J. Biochem.* **84**, 513–520 (1978).
21. T. Pánek *et al*., First multigene analysis of *Archamoebae* (*Amoebozoa*: *Conosa*) robustly reveals its phylogeny and shows that *Entamoebidae* represents a deep lineage of the group. *Mol. Phylogenet. Evol.* **98**, 41–51 (2016).
22. C. Neufeld *et al*., Structural basis for competitive interactions of Pex14 with the import receptors Pex5 and Pex19. *EMBO J.* **28**, 745–754 (2009).
23. J. Koch, C. Brocard, PEX11 proteins attract Mff and human Fis1 to coordinate peroxisomal fission. *J. Cell Sci.* **125**, 3813–3826 (2012).
24. H. Otera *et al*., Mff is an essential factor for mitochondrial recruitment of Drp1 during mitochondrial fission in mammalian cells. *J. Cell Biol.* **191**, 1141–1158 (2010).
25. C. Williams, M. van den Berg, R. R. Sprenger, B. Distel, A conserved cysteine is essential for Pex4p-dependent ubiquitination of the peroxisomal import receptor Pex5p. *J. Biol. Chem.* **282**, 22534–22543 (2007).
26. S. Goto, S. Mano, C. Nakamori, M. Nishimura, *Arabidopsis* ABERRANT PEROXISOME MORPHOLOGY9 is a peroxin that recruits the PEX1-PEX6 complex to peroxisomes. *Plant Cell* **23**, 1573–1587 (2011).
27. V. C. Kalel, P. Mäser, M. Sattler, R. Erdmann, G. M. Popowicz, Come, sweet death: Targeting glycosomal protein import for antitrypanosomal drug development. *Curr. Opin. Microbiol.* **46**, 116–122 (2018).
28. S. Galiani *et al*., Super-resolution microscopy reveals compartmentalization of peroxisomal membrane proteins. *J. Biol. Chem.* **291**, 16948–16962 (2016).
29. L. D. Barlow, E. Nývltová, M. Aguilar, J. Tachezy, J. B. Dacks, A sophisticated, differentiated Golgi in the ancestor of eukaryotes. *BMC Biol.* **16**, 27 (2018).
30. S. Bauer, J. C. Morris, M. T. Morris, Environmentally regulated glycosome protein composition in the African trypanosome. *Eukaryot. Cell* **12**, 1072–1079 (2013).
31. S. K. Banerjee, P. S. Kessler, T. Saveria, M. Parsons, Identification of trypanosomatid PEX19: Functional characterization reveals impact on cell growth and glycosome size and number. *Mol. Biochem. Parasitol.* **142**, 47–55 (2005).
32. C. Krause, H. Rosewich, A. Woehler, J. Gärtner, Functional analysis of PEX13 mutation in a Zellweger syndrome spectrum patient reveals novel homooligomerization of PEX13 and its role in human peroxisome biogenesis. *Hum. Mol. Genet.* **22**, 3844–3857 (2013).
33. T. P. Dunkley, R. Watson, J. L. Griffin, P. Dupree, K. S. Lilley, Localization of organelle proteins by isotope tagging (LOPIT). *Mol. Cell. Proteomics* **3**, 1128–1134 (2004).
34. R. Rucktäschel, W. Girzalsky, R. Erdmann, Protein import machineries of peroxisomes. *Biochim. Biophys. Acta* **1808**, 892–900 (2011).
35. J. Moyersoen, J. Choe, E. Fan, W. G. Hol, P. A. Michels, Biogenesis of peroxisomes and glycosomes: Trypanosomatid glycosome assembly is a promising new drug target. *FEMS Microbiol. Rev.* **28**, 603–643 (2004).
36. M. Helm *et al*., Dual specificities of the glyoxysomal/peroxisomal processing protease Deg15 in higher plants. *Proc. Natl. Acad. Sci. U.S.A.* **104**, 11501–11506 (2007).
37. P. A. Watkins, J. M. Ellis, Peroxisomal acyl-CoA synthetases. *Biochim. Biophys. Acta* **1822**, 1411–1420 (2012).
38. T. Annoura, T. Nara, T. Makiuchi, T. Hashimoto, T. Aoki, The origin of dihydroorotate dehydrogenase genes of kinetoplastids, with special reference to their biological significance and adaptation to anaerobic, parasitic conditions. *J. Mol. Evol.* **60**, 113–127 (2005).
39. K. Acosta-Virgen *et al*., *Giardia lamblia*: Identification of peroxisomal-like proteins. *Exp. Parasitol.* **191**, 36–43 (2018).
40. A. K. Ludewig-Klingner, V. Michael, M. Jarek, H. Brinkmann, J. Petersen, Distribution and evolution of peroxisomes in alveolates (*Apicomplexa*, Dinoflagellates, Ciliates). *Genome Biol. Evol.* **10**, 1–13 (2018).
41. A. B. Vaidya, M. W. Mather, Mitochondrial evolution and functions in malaria parasites. *Annu. Rev. Microbiol.* **63**, 249–267 (2009).
42. V. Žárský, J. Tachezy, Evolutionary loss of peroxisomes–Not limited to parasites. *Biol. Direct* **10**, 74 (2015).
43. M. Müller *et al*., Biochemistry and evolution of anaerobic energy metabolism in eukaryotes. *Microbiol. Mol. Biol. Rev.* **76**, 444–495 (2012).
44. L. L. Cross, H. T. Ebeed, A. Baker, Peroxisome biogenesis, protein targeting mechanisms and PEX gene functions in plants. *Biochim. Biophys. Acta* **1863**, 850–862 (2016).
45. N. H. Gonzalez *et al*., A single peroxisomal targeting signal mediates matrix protein import in diatoms. *PLoS One* **6**, e25316 (2011).
46. A. M. Motley, E. H. Hettema, R. Ketting, R. Plasterk, H. F. Tabak, *Caenorhabditis elegans* has a single pathway to target matrix proteins to peroxisomes. *EMBO Rep.* **1**, 40–46 (2000).
47. C. P. Grou *et al*., Members of the E2D (UbcH5) family mediate the ubiquitination of the conserved cysteine of Pex5p, the peroxisomal import receptor. *J. Biol. Chem.* **283**, 14190–14197 (2008).
48. S. Skrede, O. Halvorsen, Mitochondrial pantetheinephosphate adenylyltransferase and dephospho-CoA kinase. *Eur. J. Biochem.* **131**, 57–63 (1983).
49. A. G. Tahiliani, J. R. Neely, Mitochondrial synthesis of coenzyme A is on the external surface. *J. Mol. Cell. Cardiol.* **19**, 1161–1167 (1987).
50. S. Reumann *et al*., In-depth proteome analysis of *Arabidopsis* leaf peroxisomes combined with *in vivo* subcellular targeting verification indicates novel metabolic and regulatory functions of peroxisomes. *Plant Physiol.* **150**, 125–143 (2009).
51. I. Pracharoenwattana, J. E. Cornah, S. M. Smith, *Arabidopsis* peroxisomal malate dehydrogenase functions in β-oxidation but not in the glyoxylate cycle. *Plant J.* **50**, 381–390 (2007).
52. M. L. S. Güther, M. D. Urbaniak, A. Tavendale, A. Prescott, M. A. J. Ferguson, High-confidence glycosome proteome for procyclic form *Trypanosoma brucei* by epitope-tag organelle enrichment and SILAC proteomics. *J. Proteome Res.* **13**, 2796–2806 (2014).
53. V. D. Antonenkov, Dehydrogenases of the pentose phosphate pathway in rat liver peroxisomes. *Eur. J. Biochem.* **183**, 75–82 (1989).
54. T. Annoura, T. Nara, T. Makiuchi, T. Hashimoto, T. Aoki, The origin of dihydroorotate dehydrogenase genes of kinetoplastids, with special reference to their biological significance and adaptation to anaerobic, parasitic conditions. *J. Mol. Evol.* **60**, 113–127 (2005).
55. M. Nagy, F. Lacroute, D. Thomas, Divergent evolution of pyrimidine biosynthesis between anaerobic and aerobic yeasts. *Proc. Natl. Acad. Sci. U.S.A.* **89**, 8966–8970 (1992).
56. V. Hines, L. D. Keys, 3rd, M. Johnston, Purification and properties of the bovine liver mitochondrial dihydroorotate dehydrogenase. *J. Biol. Chem.* **261**, 11386–11392 (1986).
57. P. S. Andersen, P. J. G. Jansen, K. Hammer, Two different dihydroorotate dehydrogenases in *Lactococcus lactis*. *J. Bacteriol.* **176**, 3975–3982 (1994).
58. P. A. Michels, V. Hannaert, F. Bringaud, Metabolic aspects of glycosomes in trypanosomatidae–New data and views. *Parasitol. Today (Regul. Ed.)* **16**, 482–489 (2000).
59. T. Makiuchi, T. Nara, T. Annoura, T. Hashimoto, T. Aoki, Occurrence of multiple, independent gene fusion events for the fifth and sixth enzymes of pyrimidine biosynthesis in different eukaryotic groups. *Gene* **394**, 78–86 (2007).
60. R. Cabrera, J. Babul, V. Guixé, Ribokinase family evolution and the role of conserved residues at the active site of the PfkB subfamily representative, Pfk-2 from *Escherichia coli*. *Arch. Biochem. Biophys.* **502**, 23–30 (2010).
61. F. R. Opperdoes, J. P. Szikora, *In silico* prediction of the glycosomal enzymes of *Leishmania major* and trypanosomes. *Mol. Biochem. Parasitol.* **147**, 193–206 (2006).
62. E. E. Gill *et al*., Novel mitochondrion-related organelles in the anaerobic amoeba *Mastigamoeba balamuthi*. *Mol. Microbiol.* **66**, 1306–1320 (2007).
63. V. Y. Petrova, D. Drescher, A. V. Kujumdzieva, M. J. Schmitt, Dual targeting of yeast catalase A to peroxisomes and mitochondria. *Biochem. J.* **380**, 393–400 (2004).
64. M. M. Leger, R. M. R. Gawryluk, M. W. Gray, A. J. Roger, Evidence for a hydrogenosomal-type anaerobic ATP generation pathway in *Acanthamoeba castellanii*. *PLoS One* **8**, e69532 (2013).
65. H. J. Santos, T. Makiuchi, T. Nozaki, Reinventing an organelle: The reduced mitochondrion in parasitic protists. *Trends Parasitol.* **34**, 1038–1055 (2018).
66. W. de Souza, A. Lanfredi-Rangel, L. Campanati, Contribution of microscopy to a better knowledge of the biology of *Giardia lamblia*. *Microsc. Microanal.* **10**, 513–527 (2004).
67. W. de Souza, Special organelles of some pathogenic protozoa. *Parasitol. Res.* **88**, 1013–1025 (2002).
68. L. A. Chávez, W. Balamuth, T. Gong, A light and electron microscopical study of a new, polymorphic free-living amoeba, *Phreatamoeba balamuthi* n. g., n. sp. *J. Protozool.* **33**, 397–404 (1986).
69. M. Cáp, L. Stěpánek, K. Harant, L. Váchová, Z. Palková, Cell differentiation within a yeast colony: Metabolic and regulatory parallels with a tumor-affected organism. *Mol. Cell* **46**, 436–448 (2012).
70. S. R. Green, C. M. Moehle, Media and culture of yeast. *Curr. Protoc. Cell Biol.* **Chapter 1**, 1.6.1–1.6.12 (2001).
71. M. T. McCammon, M. Veenhuis, S. B. Trapp, J. M. Goodman, Association of glyoxylate and beta-oxidation enzymes with peroxisomes of *Saccharomyces cerevisiae*. *J. Bacteriol.* **172**, 5816–5827 (1990).
72. L. Sterck, K. Billiau, T. Abeel, P. Rouzé, Y. Van de Peer, ORCAE: Online resource for community annotation of eukaryotes. *Nat. Methods* **9**, 1041 (2012).
73. G. Neuberger, S. Maurer-Stroh, B. Eisenhaber, A. Hartig, F. Eisenhaber, Motif refinement of the peroxisomal targeting signal 1 and evaluation of taxon-specific differences. *J. Mol. Biol.* **328**, 567–579 (2003).
74. P. B. Lazarow, The import receptor Pex7p and the PTS2 targeting sequence. *Biochim. Biophys. Acta* **1763**, 1599–1604 (2006).
75. C. R. Flynn, R. T. Mullen, R. N. Trelease, Mutational analyses of a type 2 peroxisomal targeting signal that is capable of directing oligomeric protein import into tobacco BY-2 glyoxysomes. *Plant J.* **16**, 709–720 (1998).
76. J. Mikolajczyk *et al*., Small ubiquitin-related modifier (SUMO)-specific proteases: Profiling the specificities and activities of human SENPs. *J. Biol. Chem.* **282**, 26217–26224 (2007).

77. K. Malínská, J. Malínský, M. Opekarová, W. Tanner, Visualization of protein compartmentation within the plasma membrane of living yeast cells. *Mol. Biol. Cell* **14**, 4427–4436 (2003).
78. R. D. Gietz, R. H. Schiestl, Large-scale high-efficiency yeast transformation using the LiAc/SS carrier DNA/PEG method. *Nat. Protoc.* **2**, 38–41 (2007).
79. J. Schindelin *et al*., Fiji: An open-source platform for biological-image analysis. *Nat. Methods* **9**, 676–682 (2012).
80. S. Bolte, F. P. Cordelières, A guided tour into subcellular colocalization analysis in light microscopy. *J. Microsc.* **224**, 213–232 (2006).
81. F. de Chaumont *et al*., Icy: An open bioimage informatics platform for extended reproducible research. *Nat. Methods* **9**, 690–696 (2012).
82. A. Makki *et al*., Triplet-pore structure of a highly divergent TOM complex of hydrogenosomes in *Trichomonas vaginalis*. *PLoS Biol.* **17**, e3000098 (2019).
83. I. Kaurov *et al*., The diverged trypanosome MICOS complex as a hub for mitochondrial cristae shaping and protein import. *Curr. Biol.* **28**, 3393–3407.e5 (2018).
84. J. J. Smith *et al*., Transcriptome profiling to identify genes involved in peroxisome assembly and function. *J. Cell Biol.* **158**, 259–271 (2002).
85. J. Šťáfková *et al*., Dynamic secretome of *Trichomonas vaginalis*: Case study of β-amylases. *Mol. Cell. Proteomics* **17**, 304–320 (2018).
86. Y. Wang *et al*., Reversed-phase chromatography with multiple fraction concatenation strategy for proteome profiling of human MCF10A cells. *Proteomics* **11**, 2019–2026 (2011).